Molecular Therapy
Original Article

Optogenetic therapy restores retinal activity in primate for at least a year following photoreceptor ablation

Juliette E. McGregor,[1] Karteek Kunala,[1] Zhengyang Xu,[2] Peter J. Murphy,[1,2] Tyler Godat,[1,2] Jennifer M. Strazzeri,[1,3] Brittany A. Bateman,[3] William S. Fischer,[1] Keith Parkins,[1] Colin J. Chu,[4] Teresa Puthussery,[5] David R. Williams,[1,2] and William H. Merigan[1,3]

[1]Center for Visual Science, 601 Crittenden Blvd., University of Rochester Medical Center, Rochester, NY 14642, USA; [2]Institute of Optics, University of Rochester, Rochester, NY 14627, USA; [3]Flaum Eye Institute, University of Rochester, Rochester, NY 14642, USA; [4]Translational Health Sciences, University of Bristol, Bristol BS105NB, United Kingdom; [5]School of Optometry & Helen Wills Neuroscience Institute, University of California, Berkeley, CA 94720, USA

All retina-based vision restoration approaches rely on the assumption that photoreceptor loss does not preclude reactivation of the remaining retinal architecture. Whether extended periods of vision loss limit the efficacy of restorative therapies at the retinal level is unknown. We examined long-term changes in optogenetic responsivity of foveal retinal ganglion cells (RGCs) in non-human primates following localized photoreceptor ablation by high-intensity laser exposure. By performing fluorescence adaptive optics scanning light ophthalmoscopy (AOSLO) of RGCs expressing both the calcium indicator GCaMP6s and the optogenetic actuator ChrimsonR, it was possible to track optogenetic-mediated calcium responses in deafferented RGCs over time. Fluorescence fundus photography revealed a 40% reduction in ChrimsonR fluorescence from RGCs lacking photoreceptor input over the 3 weeks following photoreceptor ablation. Despite this, *in vivo* imaging revealed good cellular preservation of RGCs 3 months after the loss of photoreceptor input, and histology confirmed good structural preservation at 2 years. Optogenetic responses of RGCs in primate persisted for at least 1 year after the loss of photoreceptor input, with a sensitivity index similar to optogenetic responses recorded in intact retina. These results are promising for all potential therapeutic approaches to vision restoration that rely on preservation and reactivation of RGCs.

INTRODUCTION

The benefits of even the most successful therapeutic approaches to restoring retinal function will be limited if post-receptoral visual processing is not preserved after photoreceptor degeneration. A complete understanding of the post-receptoral sequelae of photoreceptor loss in humans is not yet available, though there is evidence that deleterious changes can occur, including retinal remodeling,[1] changes to subsequent stages of the visual pathway including white matter[2] and cortex,[3] and extensive evidence that visual function does not recover fully after long-term deprivation.[4]

A prerequisite for restoring vision at the retinal level via any therapeutic intervention is that the target cell classes remain stable in the deafferented retina. This requirement is most challenging for photoreceptor replacement therapies, sub-retinal implants, and bipolar cell-targeted optogenetics, as there is evidence of extensive remodeling at the bipolar cell level.[5] Optogenetic therapy targeting retinal ganglion cells (RGCs) may be advantageous, as the inner retina appears to be relatively more stable after photoreceptor loss,[1] although how stable remains controversial. In rodent models variable degrees of RGC loss and structural remodeling have been reported, ranging from good structural preservation[6,7] to moderate RGC loss[8] and catastrophic RGC death and extensive inner retinal remodeling.[9] These conflicting data may reflect differences in the time point analyzed, the retinal degeneration model, or the methodology used.

In human, data on RGC death and structural remodeling has been observed in moderate- to late-stage retinitis pigmentosa (RP) and age-related macular degeneration (AMD) patients.[10,11] One study observed a 70% loss of RGCs in RP,[12] while histology in remaining RGCs showed structural indicators of organelle stress and autophagy.[1] The natural history of progression of these diseases means that photoreceptor function may have been lost many years prior to tissue examination. These data suggest that understanding the time window over which intervention is possible may be critical for the efficacy of vision restoration therapies.

Physiologically, rodent models of retinal degeneration have also shown aberrant firing patterns in RGCs including enhanced intrinsic

Received 22 April 2021; accepted 14 September 2021;
https://doi.org/10.1016/j.ymthe.2021.09.014.

Correspondence: Juliette E. McGregor, Center for Visual Science, University of Rochester Medical Center, Rochester, NY 14642, USA.
E-mail: jmcgrego@ur.rochester.edu
Correspondence: William H. Merigan, Center for Visual Science, 601 Crittenden Blvd., University of Rochester Medical Center, Rochester, NY 14642, USA.
E-mail: wmerigan@ur.rochester.edu

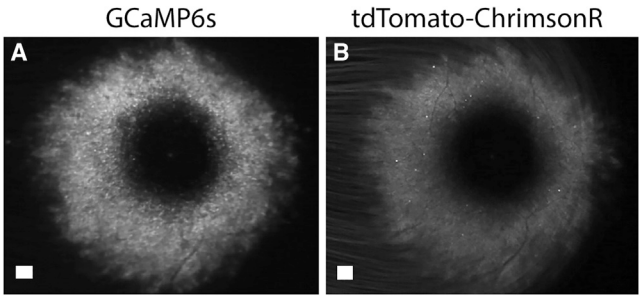

Figure 1. Fluorescent GCaMP and tdTomato-ChrimsonR expression in the ring of RGCs that serve the central fovea of the macaque

(A) Fluorescence fundus image of GCaMP expression in primate fovea 4.5 months after injection of the viral vector and 2 days prior to photoreceptor ablation. (B) Fluorescence fundus image of ChrimsonR-tdTomato expression in primate fovea 4.5 months after injection of the viral vector and 1 week prior to photoreceptor ablation. All scale bars 100 μm. All data taken in animal 1. Data from animal 2 shown in Figure S1.

excitability and increased spontaneous firing and changes in membrane permeability, gene transcription, and protein distribution.[8,13–15] Whether these changes take place in the adult primate and the extent to which they impair the quality of restored vision is currently unknown.

We recently developed an *in vivo* adaptive optics imaging technique that allowed us to demonstrate optogenetic restoration of RGC function in the living primate.[16] Calcium imaging adaptive optics scanning light ophthalmoscopy (AOSLO) allows us to longitudinally assess the function of individual RGCs after photoreceptor ablation, providing a way to examine whether photoreceptor loss produces retinal changes that might compromise the benefits of optogenetic vision restoration.

In this study, we use an acute photoreceptor ablation approach[17] to create a micro-scotoma in the adult primate, depriving a subset of foveal RGCs of their photoreceptor input. We use fluorescence fundus imaging and structural and functional AOSLO to follow optogenetic expression and responsivity of RGCs with and without photoreceptor input for 12 weeks after photoreceptor ablation and in a second animal demonstrate that optogenetic-mediated RGC activity persists for at least 12 months after the loss of photoreceptor input. Consistent with these physiological findings, optical coherence tomography (OCT) and histological examination of the deafferented fovea 2 years after photoreceptor ablation also suggest that the ganglion cell layer (GCL) was well preserved.

RESULTS

Co-expression of the fluorescently labeled optogenetic actuator ChrimsonR-tdTomato and the fluorescent calcium indicator GCaMP6s

Long-term expression of the optogenetic actuator ChrimsonR and the calcium indicator GCaMP6s was achieved by intravitreal co-injection of AAV2-*CAG-ChrimsonR:tdTomato* and AAV2-*CAG-GCaMP6s* (detailed in Table S2) into one female (animal 1) and one male (animal 2) macaque that had received immune suppression with cyclosporine prior to injection. Transgene expression was observed by fluorescence fundus and confocal scanning laser ophthalmoscope (cSLO) imaging of GCaMP and tdTomato 2 weeks after the injection in both animals. Ocular inflammation was observed at 7 weeks (animal 1) and 3 weeks (animal 2), as detailed in Table S1. In both cases, this resolved after treatment with intravitreal steroid injection. I*n vivo* fundus images of ChrimsonR-tdTomato and GCaMP6s expression in foveal ganglion cells are shown 4.5 months (animal 1, Figure 1) and 1 year (animal 2, Figure S1) after injection of the viral vectors and 12 and 4 days prior to photoreceptor ablation, respectively. The ring of foveal expression in the GCL is consistent with previous studies.[18,19]

Localized high-power pulsed IR laser exposure created a localized region of deafferented RGCs in primate fovea

At the fovea, RGC somas are laterally displaced from the photoreceptors that drive them. To remove photoreceptor input to RGCs in the temporal region of the fovea, a localized, high-power ultrafast near infrared (NIR) laser exposure was delivered temporal to the central foveola (shown schematically in black in Figure 2A). OCT data taken 2 days after photoreceptor ablation in animal 1 show localized disruption to the photoreceptor layer (PRL) in the foveola (Figure 2B). The structure of the retina under the ganglion cell ring on both sides of the fovea appears normal. AOSLO (NIR) reflectance imaging of the fovea 2 h after delivery of a high-power ultrashort NIR exposure shows disruption to the photoreceptor layer and radial Henle fibers (Figure 2C) connecting the ablated photoreceptors to their bipolar cells and then RGCs, which are radially displaced at the fovea.

Photoreceptor ablation at the foveola caused an abrupt reduction in GCaMP fluorescence in RGCs in a spatial pattern consistent with the loss of photoreceptor input to these cells (Figure 2D). Fluorescent fundus images taken 2 days after photoreceptor ablation show a 71% decrease in fluorescence intensity in this region relative to the same location prior to the lesion. Similar results were obtained in a second animal (animal 2) shown in Figure S1. The spatial displacement between the photoreceptors and the RGCs cells they are connected to ensures that this change is not due to direct damage by laser exposure but rather due to the loss of photoreceptor afferents. Low-intensity, 0.45-Hz flicker drove 0.45-Hz photoreceptor-mediated calcium responses in RGCs with photoreceptor afferents intact (Figure 2G) but not in RGCs at an eccentricity-matched location with receptive fields exposed to the high-power pulsed laser source (Figure 2F), confirming that photoreceptor input to RGCs had been lost.

tdTomato-ChrimsonR and GCaMP fluorescence decreased over a 6-week period in deafferented RGCs

Adaptive optics NIR reflectance imaging focused at the photoreceptor layer 2 h after the exposure showed darkening consistent with a loss of waveguiding in foveal cones presumably due to cell loss, inflammation, and misorientation (Figure 3A). Photoreceptors on the edge of the ablated zone appear to begin waveguiding again by day 13 and brighten further to week 3, possibly as any edema or inflammation

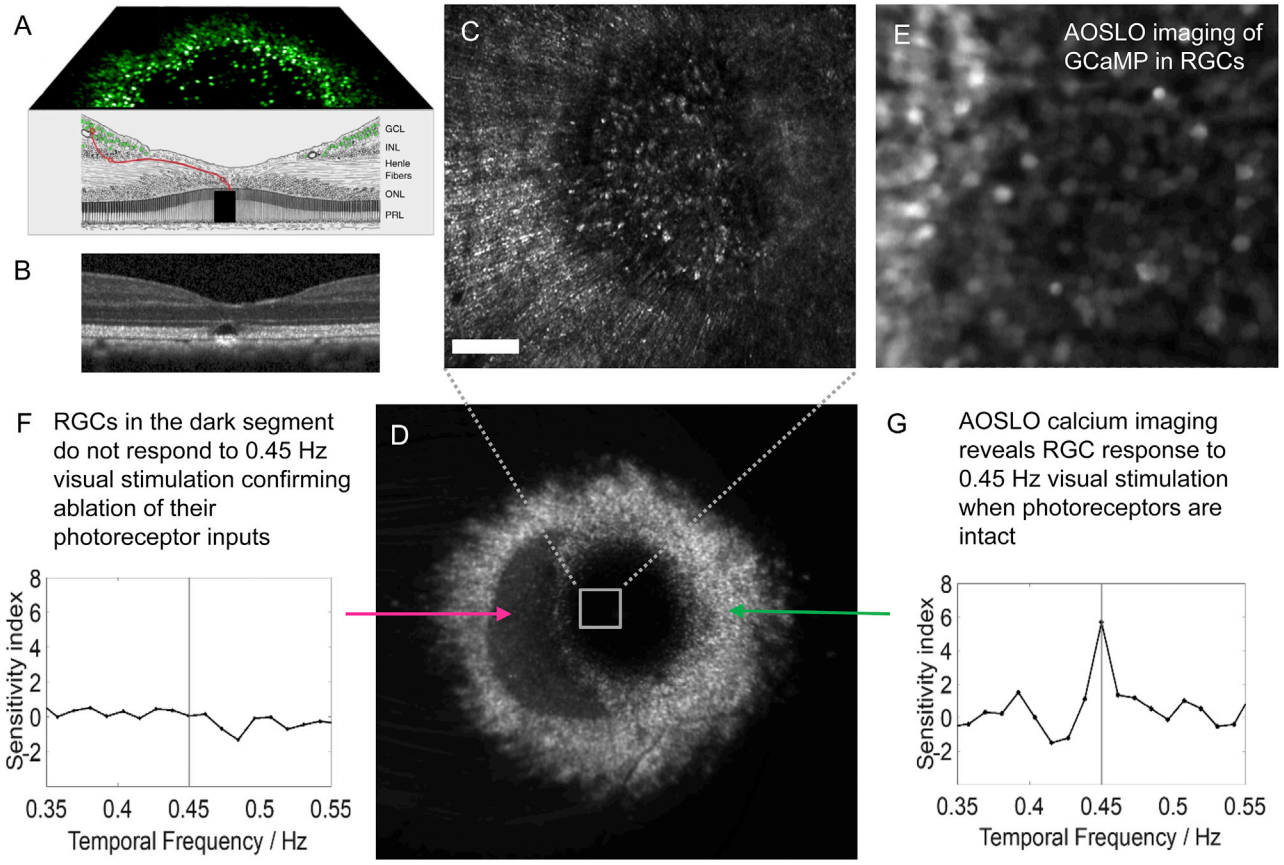

Figure 2. Creation and *in vivo* testing of micro-scotomas in primate fovea

(A) Schematic diagram of the fovea showing target location of photoreceptor ablation in foveola and displaced foveal RGCs. (B) OCT image through the region of fovea subjected to high-intensity ultrafast laser exposure showing localized ablation of PRL. (C) AOSLO NIR reflectance image of the exposed region 2 h after exposure; note Henle fibers visible. Scale bar, 100 μm. (D) cSLO image of the GCaMP fluorescence of foveal RGCs 2 days after photoreceptor ablation, with dark segment representing RGCs whose photoreceptor input has been ablated (data also shown in Figure 3E). Scale bar, 100 μm. (E) Fluorescence AOSLO image of GCaMP expressing RGCs at the boundary of the dark segment 2 h after photoreceptor ablation. Scale bar, 50 μm. (F) No GCaMP response to 0.45-Hz visual stimulation of the central foveal cones is observed from RGCs in the dark segment 2 weeks after photoreceptor ablation, supporting the loss of photoreceptor input to these cells. (G). A clear 0.45 Hz response is observed from RGCs on the right of the foveal ring driven by intact foveal photoreceptors at the same time point as (F). Data from animal 1.

subsides (Figures 3B–3D). Figures 3E–3H show the region of reduced RGC fluorescence over time. The dimmed segment of RGCs contracts slightly between the day of the lesion and day 10, consistent with the reduction in the apparent size of the disrupted photoreceptor layer. The area of reduced fluorescence appears relatively stable from week 3 to week 12. Resting GCaMP fluorescence within the dimmed zone decreases over the 6 weeks immediately following photoreceptor ablation in the region that has lost photoreceptor input (Figure 3I).

To visualize the optogenetic actuator ChrimsonR *in vivo*, the transgene included a sequence coding for the fluorescent protein tdTomato. Fluorescent fundus imaging with filters to exclude GCaMP fluorescence was used to track ChrimsonR-tdTomato fluorescence over time after photoreceptor ablation (Figures 3J–3M). In contrast to GCaMP fluorescence, levels of tdTomato fluorescence did not change abruptly after the ultrafast laser exposure. However, over the following 3 weeks, mean tdTomato fluorescence in deafferented RGCs was reduced by 40% relative to an eccentricity-matched region with photoreceptor input intact. From week 3 onward, tdTomato fluorescence remained relatively stable until the end of the 18-week monitoring period (Figure 3M). Barring changes in fluorescence quenching in deafferented cells, since tdTomato and ChrimsonR are expressed together, we can infer that ChrimsonR levels also reduced by 40% in the 3 weeks following photoreceptor ablation and then stabilized. A similar 40% reduction in tdTomato fluorescence was observed in deafferented RGCs of animal 2 (Figure S1).

AOSLO imaging shows good preservation of RGC cellular structure 3 months after photoreceptor ablation

Adaptive optics imaging of both the GCaMP and tdTomato signals allowed structural observation of the RGCs lacking photoreceptor input at a cellular scale. tdTomato and ChrimsonR are expressed in the cell membrane, whereas GCaMP6s is cytosolic. Figure 4 shows an adaptive optics montage of tdTomato signal from RGCs 3 months

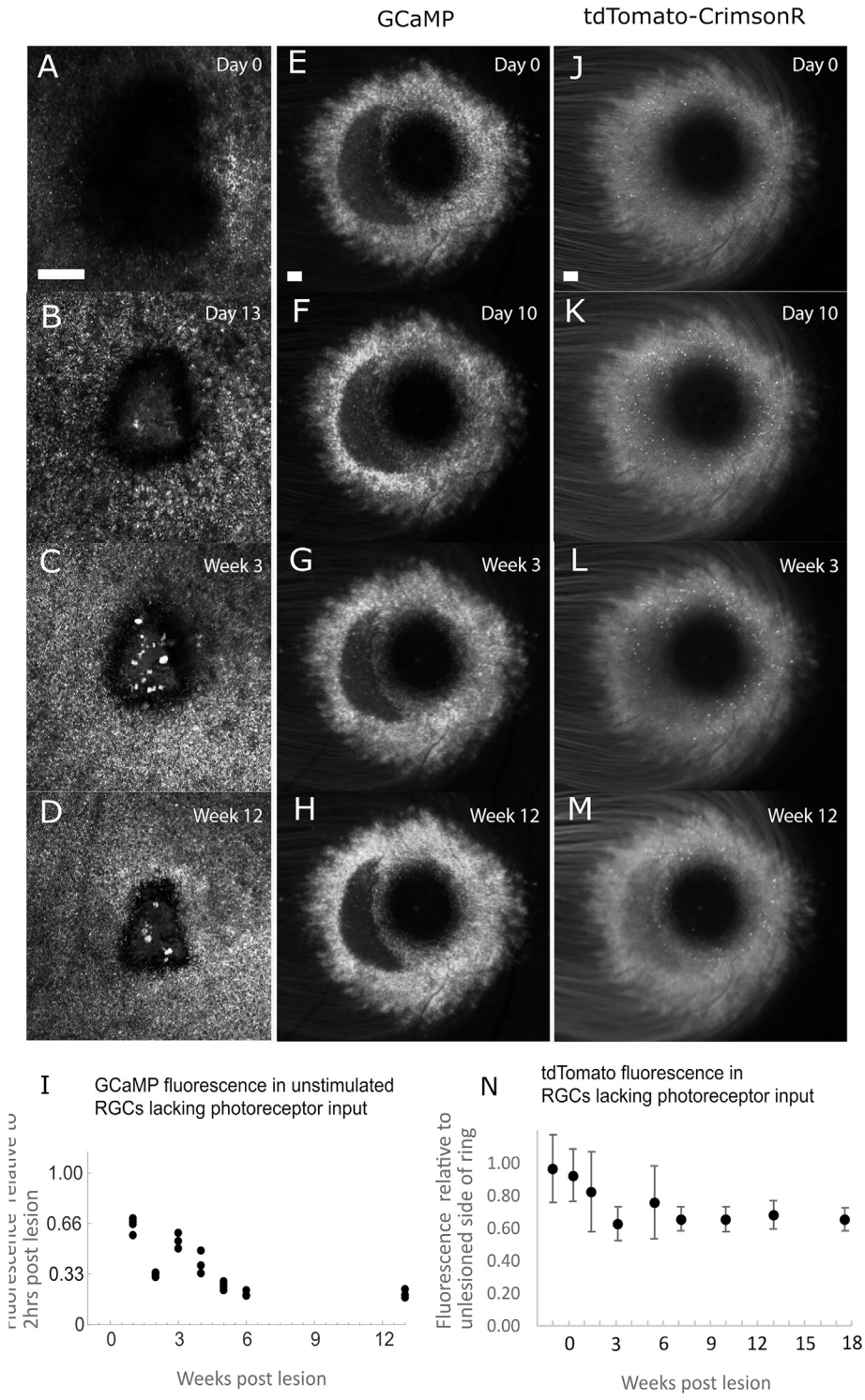

Figure 3. *In vivo* imaging of retinal changes in the weeks immediately following photoreceptor ablation

(A–D) AOSLO NIR reflectance images of ablated photoreceptor layer over time. (E–H) Fluorescence fundus images of GCaMP expression in primate over time after localized photoreceptor ablation close to vertical meridian. (I) GCaMP Fluorescence in deafferented RGCs over time. (J–M) Fluorescence fundus images of ChrimsonR-tdTomato over time after localized photoreceptor ablation. (N) tdTomato fluorescence in deafferented RGCs relative to an eccentricity-matched location with photoreceptor afferents intact. Error bars SD. All scale bars 100 μm. All data taken in animal 1. Data from animal 2 shown in Figure S1.

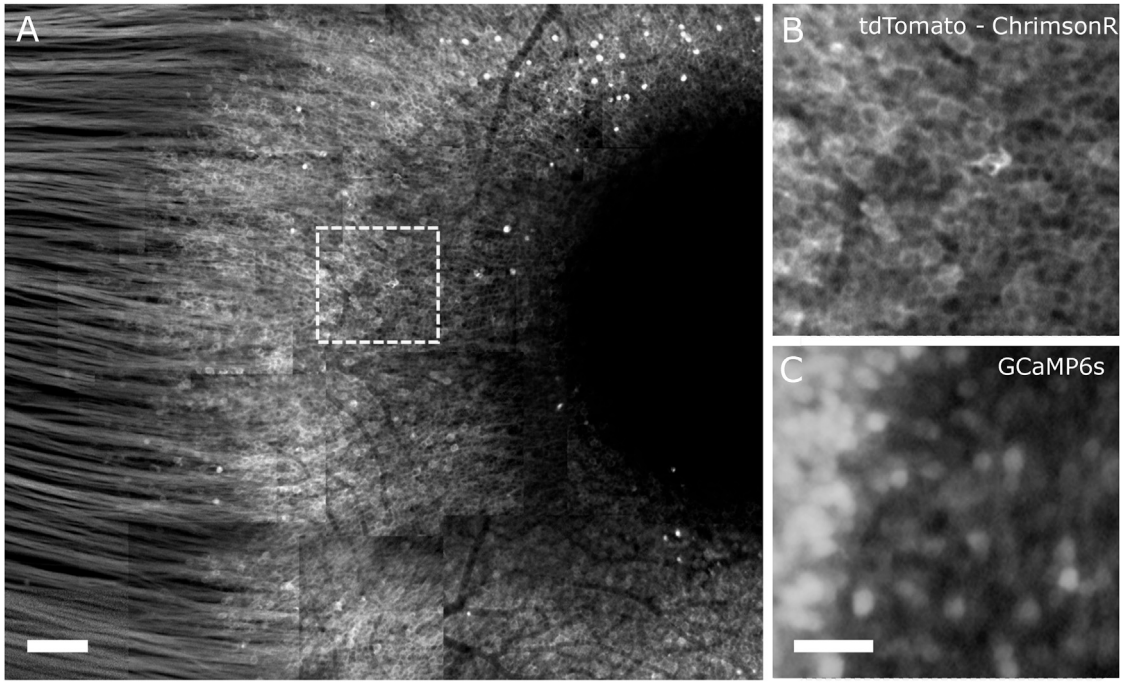

Figure 4. Cellular scale AOSLO imaging of deafferented RGCs *in vivo*

(A) AOSLO montage of tdTomato-ChrimsonR 3 months after photoreceptor ablation. Scale bar, 100 μm. (B) High-resolution tdTomato AOSLO image taken with a 1.5 Airy disk pinhole, corresponding to region in dashed box in (A). Scale bar as shown in (C). (C) GCaMP AOSLO image of the same region shown in (B) recorded with an 8 Airy disk pinhole. Scale bar, 50 μm. Data from animal 1.

after ablation of their receptive fields together with expanded panels showing the cellular structure in an area on the boundary of normal and deafferented RGCs (Figure 4A, dashed box) imaged with both tdTomato (Figure 4B)- and GCaMP (Figure 4C)-selective filters. The bright region of cells in Figure 4C corresponds to RGCs that have photoreceptor input intact. There are no striking changes in the cellular structure associated with the loss of photoreceptor input; rather, the expression of tdTomato appeared reduced.

The sensitivity index of optogenetic-driven calcium responses in deafferented RGCs is higher than in light-adapted RGCs in the 6 weeks following photoreceptor ablation but decreases to parity by week 13

By co-expressing both the optogenetic actuator ChrimsonR and the calcium indicator GCaMP6s in the same RGCs, it was possible to both optically stimulate and read out restored RGC function over time. Sixty-eight cells were segmented from images of the region of RGCs deprived of photoreceptor input by laser ablation (Figures 5A and 5B) and 76 cells in an eccentricity-matched region of the RGC ring with photoreceptor input intact (Figures 5B and 5C). RGCs were optogenetically stimulated by a 640-nm, 0.45-Hz drifting grating focused on the GCL (Figure 5B). In light of changing levels of GCaMP expression, the response was characterized with the sensitivity index (Figure 5D), which scales the response at 0.45 Hz by the standard deviation of the noise, giving a detectability metric that is independent of absolute fluorescence.

The mean sensitivity index for both the region with photoreceptor input removed and the region with photoreceptor input intact was depressed at the first data point 2 h after photoreceptor ablation (week zero), potentially a reflection of the edema and inflammation associated with retinal trauma. For the first 6 weeks after photoreceptor loss, optogenetic responsivity, as characterized by the sensitivity index, was greater in deafferented RGCs than in RGCs with photoreceptors intact. This may reflect differences in calcium activity in light-adapted cells with a maintained discharge versus those with no photoreceptor activity. Over the 3-month observation period, mean sensitivity index decreased ~2-fold in the deafferented RGCs relative to the weeks immediately following photoreceptor ablation, such that by week 13 the mean sensitivity index of deafferented and intact RGCs were similar. The sensitivity index data reported in Figure 5D were computed using the Fourier component of the signal at the frequency of interest (Figure 5E) and the standard deviation of the noise in the Fourier transform (Figure 5F). The absolute signal at the optogenetic stimulation frequency decreased in deafferented RGCs over the first 6 weeks, in a similar manner to the reduction in absolute GCaMP fluorescence (F0, the first Fourier component representing the static brightness) observed in Figure 3I.

One year after photoreceptor ablation, deafferented RGCs show optogenetic responses with a sensitivity index similar to optogenetic responses in intact retina

ChrimsonR-mediated responses to a 0.45-Hz drifting grating were recorded at 1 year (Figures 6A and 6B) and in a second animal (animal

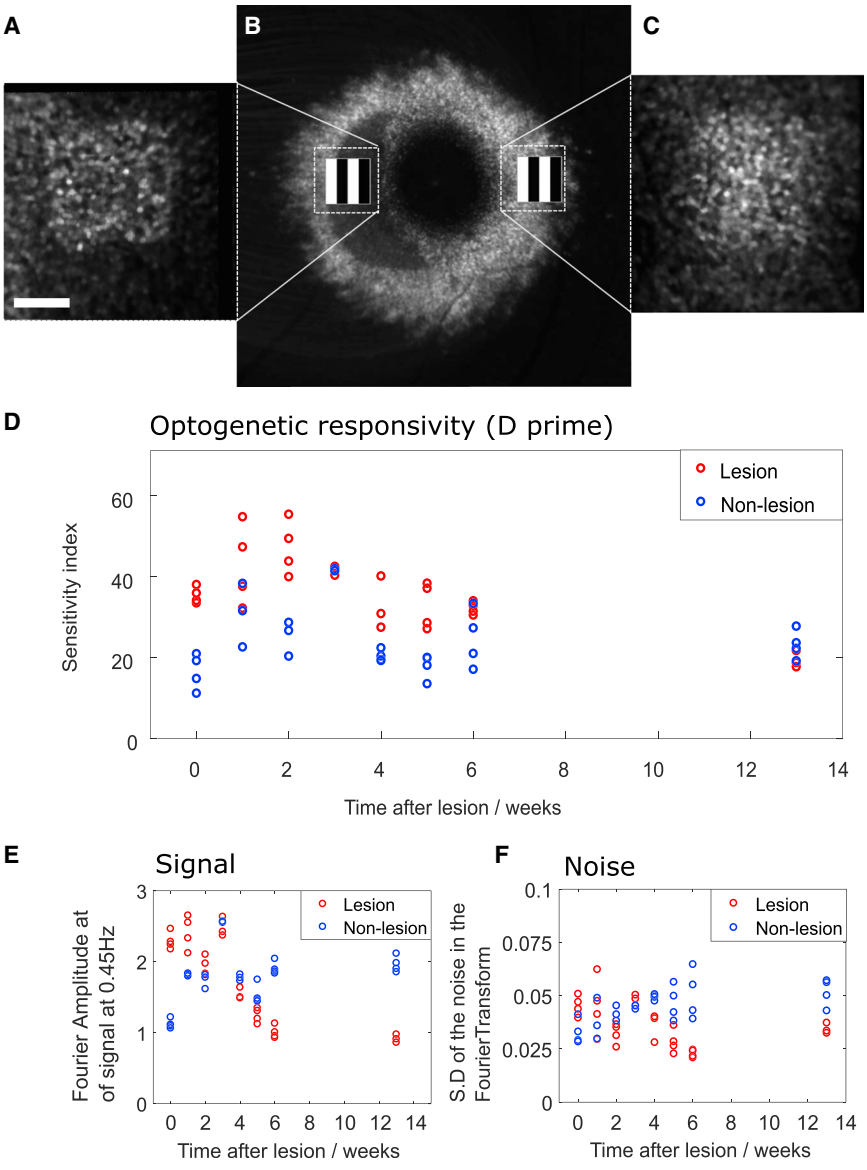

Figure 5. RGC responses to optogenetic stimulation were recorded by calcium imaging AOSLO in the 3 months following photoreceptor ablation

(A and C) AOSLO images of GCaMP-expressing RGCs with photoreceptor input removed and photoreceptor input intact, respectively. Scale bar, 100 μm. (B) cSLO image showing GCaMP fluorescence in the whole foveal RGC ring with AOSLO imaging locations shown. (D) Mean sensitivity index of the responses of 68 RGCs lacking photoreceptor input and 76 RGCs with photoreceptor input intact during each 90-s optogenetic stimulation trial over a 13-week period following photoreceptor ablation in RGCs lacking photoreceptor input (red) and with photoreceptor input intact (blue). (E) Absolute magnitude of Fourier component at the optogenetic stimulation frequency for lesioned (red) and non-lesioned (blue) RGCs shown in (D). (F) Absolute standard deviation of the noise in the Fourier transform in unstimulated frequency bands under 1 Hz excluding the stimulation frequency, respiration frequency, and harmonics. All data taken in animal 1.

2) that had undergone photoreceptor ablation 1 year previously (Figures 6C–6G). In this case we compared cells that had lost photoreceptor input and those that had not within the same adaptive optics field of view. Despite an extended period of 1 year without photoreceptor activation, RGCs showed restored responses with a sensitivity index similar to those with photoreceptor input intact.

Foveal GCL is well preserved 2 years after photoreceptor ablation

To assess the impact of photoreceptor ablation on the structural integrity of the inner retina 2 years post-ablation, we examined the integrity of the GCL by cSLO, OCT, and histology (Figure 7). The loss of activity-dependent GCaMP fluorescence in RGCs temporal to the lesion was evident with *in vivo* cSLO, reflecting the loss of photoreceptor input to these RGCs. With OCT examination, no gross structural changes were observed in the GCL on the lesioned side of the fovea (temporal) compared to the unlesioned side (nasal, Figures 7B–7D). The gross integrity of the GCL and inner nuclear layer (INL) and the region of photoreceptor ablation was confirmed histologically with toluidine blue-basic fuchsin staining (Figure 7E). With fluorescence microscopy, co-expression of GCaMP and ChrimsonR (inset in Figure 7F) was still present 3 years after the intravitreal co-injection of viral vectors in this animal, and ChrimsonR expression was evident in both On- and Off-RGCs (Figure 7F). We used an antibody for cone arrestin to visualize the site of photoceptor ablation (Figure 7G). This staining revealed an ∼100-μm-wide lesion at the level of the photoreceptor outer and inner segments in a region just temporal to the center of the foveola. To delineate the extent of the outer plexiform layer (OPL) deafferented by the lesion, we immunolabeled for vesicular glutamate transporter 1 (VGLUT1), a protein expressed in photoreceptor synaptic terminals (Figure 7H). The loss of VGLUT1 staining in the temporal OPL demarcates the region deafferented by the lesion and corresponds well with the lateral extent of the functionally deafferented zone in Figure 7A (∼440 μm). Note that the lateral displacement of the deafferented zone from the lesion site is expected from the anatomical organization of the fovea (see Figure 2A). 80% of the displacement between photoreceptors and RGCs is the Henle fiber length,[20] and thus the RGCs that have lost photoreceptor input do not extend beyond the imaged field of view in Figure 7H. Finally, we used the specific RGC marker RPBMS[21] to compare the structural integrity of RGCs

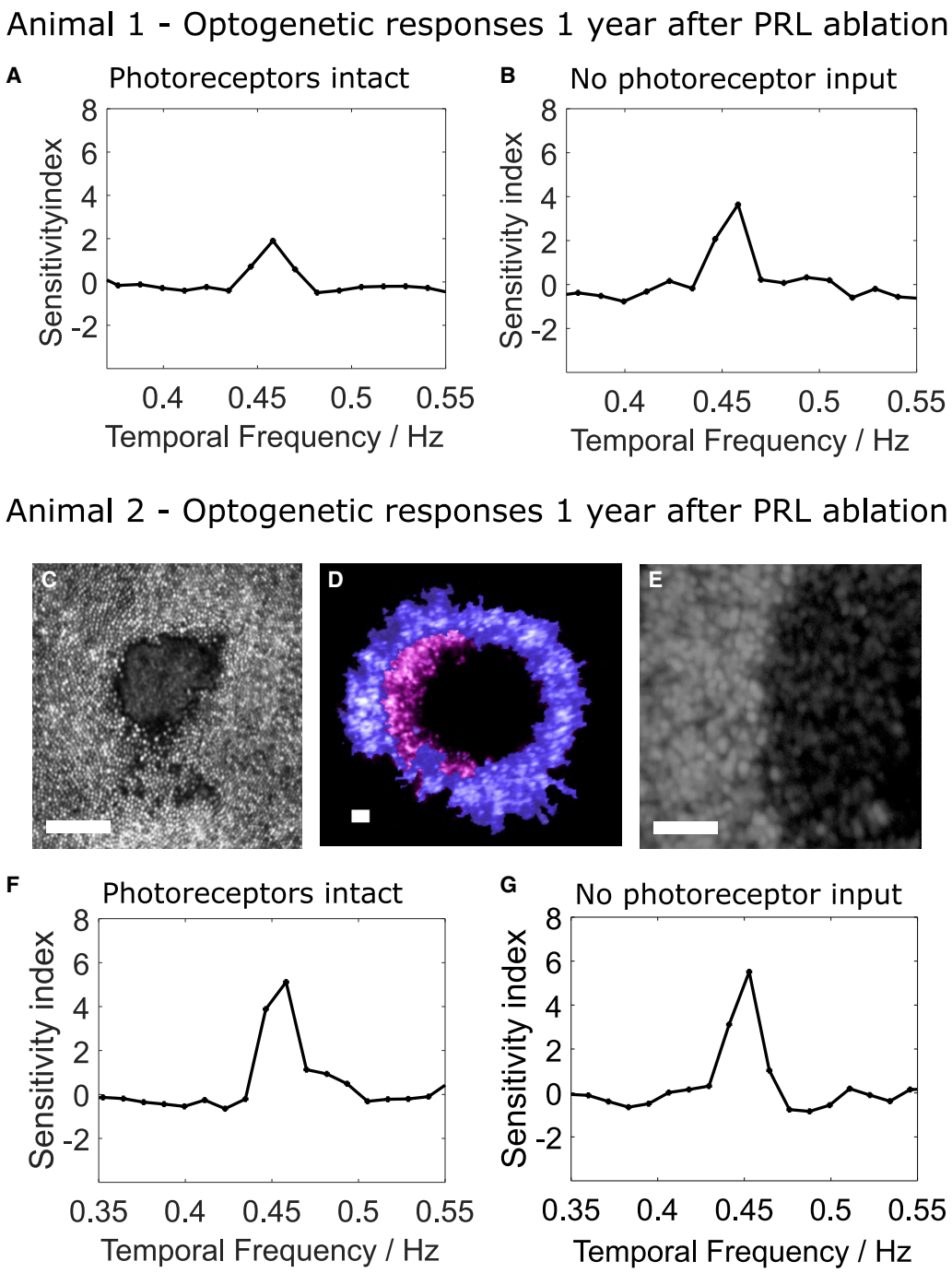

Figure 6. ChrimsonR-mediated activity persists in RGCs 1 year after photoreceptor ablation

(A) Optogenetic response to 0.45-Hz stimulation in RGCs whose photoreceptor input was removed 1 year prior to recording (animal 1, *in vivo* imaging shown in Figures 1, 2, 3, 4, and 5). Scale bar, 100 μm. (B) Optogenetic response to 0.45-Hz stimulation in cells recorded simultaneously in the same field of view but with photoreceptor input intact (animal 1). (C) Reflectance image of photoreceptor mosaic at foveola 1 year after ablation in animal 2. Scale bar, 100 μm. (D) Colorized cSLO image showing region of RGCs with photoreceptor input removed (pink) in animal 2. (E) Logarithmically scaled AOSLO GCaMP fluorescence image containing both bright RGCs with photoreceptor input intact and dim RGCs without photoreceptor input (animal 2). Scale bar, 100 μm. (F) Optogenetic response to 0.45-Hz stimulation in RGCs whose photoreceptor input was removed 1 year prior to recording, in animal 2. (G). Optogenetic response to 0.45-Hz stimulation in cells recorded simultaneously in the same field of view but with photoreceptor input intact in animal 2.

in the deafferented region (temporal, Figure 7I1) with those at the equivalent eccentricity on the non-lesioned side of the foveola (nasal, Figure 7I2) and found no qualitative differences. These histological data, taken together with the *in vivo* imaging data, show that the GCL remains structurally well preserved 2 years after photoreceptor ablation.

DISCUSSION

We have demonstrated that optogenetic reactivation of RGCs can be maintained for at least 1 year after photoreceptor ablation in two adult primates. This is promising for all forms of vision restoration that rely on reactivation of RGCs after photoreceptor degeneration. This result, together with our AOSLO data showing normal cellular structure 3 months after deafferentation and our finding of good histological preservation of the GCL 2 years after photoreceptor ablation, was surprising and encouraging, given the profound disorganization of inner retina that has been reported to follow loss of photoreceptor input.[1]

Severe remodeling has been reported in very advanced stages of retinal degeneration in human patients as well as in many models of rodent retinal degeneration, results that contrast with the findings reported here. It is possible that in our laser damage model insufficient time has elapsed relative to progressive photoreceptor loss occurring in naturally occurring retinal degenerations that would ultimately lead to substantial RGC death. Rapid disorganization of inner retina (60 days) after insult was reported in a rodent study of laser-lesioned retina;[9] however, both the model animal and the laser damage paradigm were very different, possibly explaining the differing outcomes. In our study RGC somas were not directly exposed to the high-energy laser when their photoreceptor receptive fields were ablated because at the primate fovea the RGC cell bodies are laterally displaced hundreds of microns relative to the photoreceptors that drive them. This allows us to remove the possibility of any direct laser damage to the RGCs and is a unique advantage of primate fovea. Furthermore, by using an ultrafast NIR later focused through an AO system, our laser damage approach generates axially confined lesions. We have previously demonstrated that even in areas of the primate retina where photoreceptor ablation was performed under overlying RGCs, their function was not impaired.[17]

In contrast to much of the remodeling literature, in the present study the therapeutic ChrimsonR was present before photoreceptor ablation and was periodically stimulated for the purposes of this study. Although experimental optogenetic activation was for no more than 15 min during relatively infrequent imaging sessions, this could have been sufficient to preclude remodeling that might be driven in part by loss of visually driven activity in inner retina. Were this the case, we would expect to see regional differences within the segment of deafferented RGCs between the square area that was stimulated and the regions that were not. No differences of this kind were observed in the tdTomato montage in Figure 4. It is also possible that the optogenetic actuator was activated by ambient light; however, this is relatively unlikely given the low sensitivity of ChrimsonR. Further studies to establish whether early optogenetic intervention does delay or reduce morphological remodeling of inner retina might shed further light on the optimum timing for therapeutic interventions to restore vision at the retinal level.

We observed a reduction of ChrimsonR-tdTomato fluorescence in primate RGC cell membranes over a 3-week period following the loss of photoreceptor input to these cells. Although we cannot exclude the possibility that fluorescence was quenched differently in deafferented versus intact retina, this observation is consistent with reports in rat of reduced melanopsin expression and transport in RGCs when acute photoreceptor degeneration was induced by *N*-methyl-*N*-nitrosourea (MNU).[14,22] We also observed a reduction in cytosolic GCaMP fluorescence over time, suggesting that changes in protein expression and trafficking were not specific to the optogenetic actuator and may reflect more general alterations in cell biology, e.g., increased autophagy of proteins. The mechanism leading to reduced ChrimsonR-tdTomato fluorescence was not explored in this study, and further work is needed to understand to what extent potential changes in protein expression and trafficking occurring in adult primate RGCs in the weeks immediately after photoreceptor loss impact the quality of restored vision.

Consistent with a reduction in the numbers of GCaMP molecules in each cell, the absolute magnitude of the calcium signal evoked by optogenetic stimulation was reduced in deafferented RGCs. Interestingly, the discriminability of optogenetic responses (d primed) of deafferented RGCs was initially higher than RGCs with normal photoreceptor input. One interpretation of this rise is that the photoreceptor response to the photopic 488-nm imaging light reduces the gain in adapted RGCs with intact photoreceptor afferents. By contrast, RGCs lacking photoreceptor input are essentially dark adapted, and the same magnitude of optogenetic stimulation may generate a more substantial calcium signal in these cells. Over the 3 months following photoreceptor ablation, we observed an ~2-fold reduction in the sensitivity index of optogenetic-mediated responses in deafferented cells, resulting in the sensitivity index of responses to optogenetic stimulation in deafferented and normal RGCs being approximately equal by 3 months. Similar results were obtained at 1 year in this and an additional monkey. How this translates into optogenetic-mediated visual performance at threshold in deafferented and intact regions of the GCL remains unexplored, but the retinal foundations for vision appear to be present.

Previous studies in mouse and rat have revealed spontaneous hyperactivity in RGCs lacking photoreceptor input.[6,13,15,23,24] One might expect that hyperactivity, if present in primate, would be observed as an increase in the noise used to compute the sensitivity index D′ (shown in Figure 5F). Although we do not observe this, it is possible that when the absolute noise is rescaled to account for decreasing GCaMP expression, increased spontaneous activity may be driving the reduction in optogenetic responsivity, and this will be the focus of future work. An additional consideration is that our approach has limited temporal bandwidth to capture this

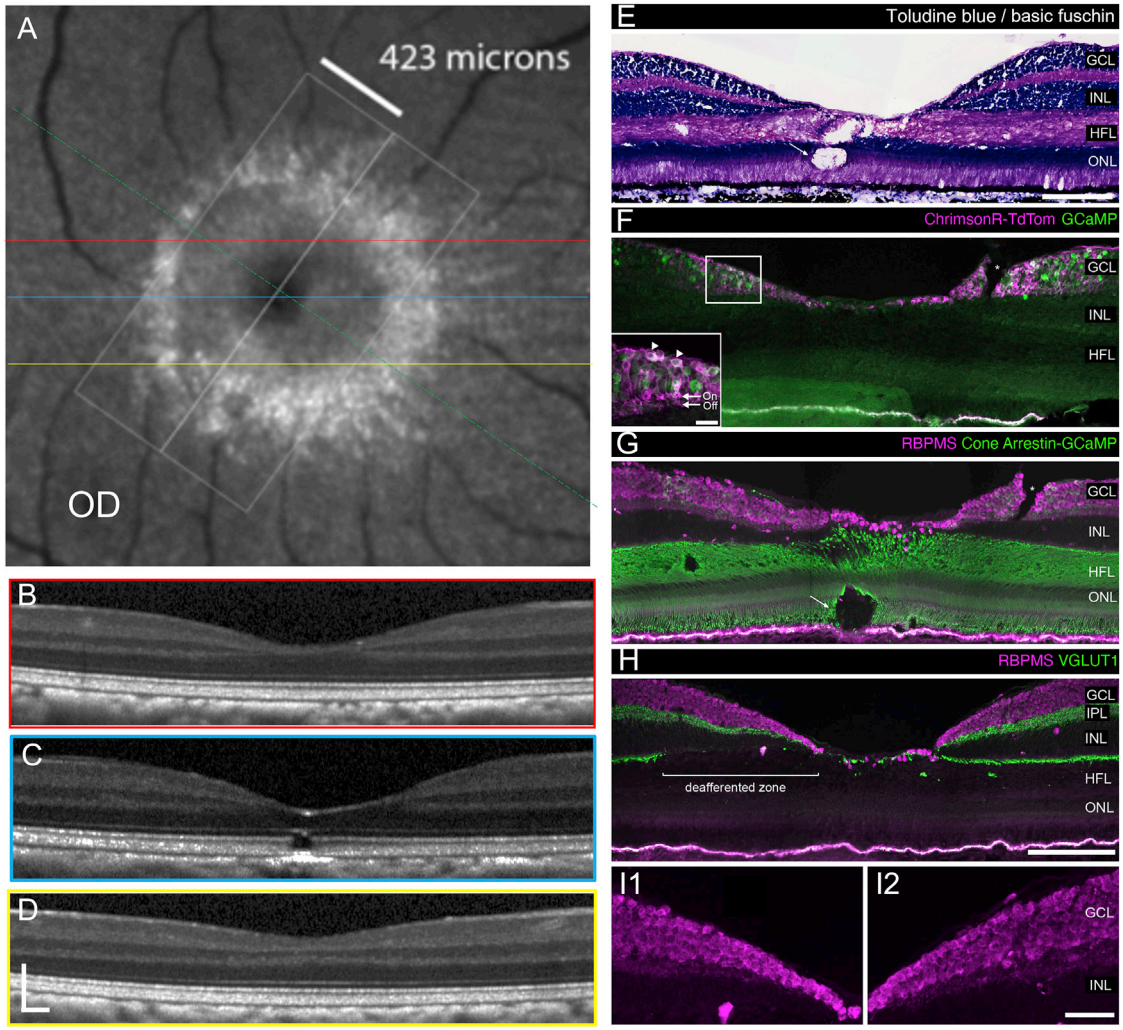

Figure 7. Structural evaluation of fovea *in vivo* and *ex vivo* 2 years after photoreceptor ablation and 3 years after the onset of ChrimsonR-tdTomato and GCaMP expression

(A) Blue autofluorescence cSLO image of the fovea of animal 2 with foveolar lesion 2 years after photoreceptor ablation. The loss of photoreceptor-mediated RGC activity reduces the GCaMP signal temporal to the photoreceptor lesion. (B–D) OCT images taken at locations through the fovea marked in (A). Scale bar, 150 μm. (E) A section stained with toluidine blue/basic fuchsin from the same animal in (A–D) showing the laser lesion site (arrow) and relative preservation of the inner retinal layers. (F) Confocal micrograph showing GCaMP and ChrimsonR-tdTomato (tdTom) fluorescence in foveal RGCs. The rectangular region of interest (ROI) is shown at higher magnification (lower left inset) to show examples of RGCs co-expressing ChrimsonR-tdTomato and GCaMP (arrowheads) and ChrimsonR-tdTomato expression in both Off- and On-RGC dendrites in the IPL (arrows). (G) The zone of photoreceptor ablation can be seen as an absence of cone arrestin labeling in the foveolar PRL (arrow). Ganglion cells in the GCL are visualized with RBPMS. (H) Loss of VGLUT1 labeling in the OPL temporal to the lesion demarcates the inner retinal region that has been deafferented. This section is from within ~60–100 μm of the section shown in (F). Note the lateral displacement of the deafferented region from the lesioned PRL due to the Henle fibers. (I) Same section as in (G) showing RBPMS-labeled RGCs in a region subjected to deafferentation (I1) and with normal photoreceptor input (I2). Scale bar in (G) applies to (E–G), 200 μm. Scale bar in (H), 50 μm. Scale bar in inset of (F), 20 μm. Asterisks show cutting artifact.

phenomenon. GCaMP6s has a long time constant of 0.6 s, making it challenging to observe spontaneous oscillations above 1 Hz. In mouse, the beating frequency of spontaneous firing has been reported in the range 3–10 Hz depending on the age of the animal.[6] To examine changes in spontaneous activity it would be desirable to deploy a faster sensor of neuronal activity or a ratiometric indicator that would allow changes in expression to be distinguished from changes in activity occurring at frequencies above the Nyquist sampling limit. If the hyperactivity observed in rodent is triggered by a diffusive signal such as retinoic acid release from retinal pigment epithelium (RPE) after photoreceptor loss,[25] it is also possible that RGCs in this study were protected by the lateral displacement between foveal RGCs and the zone of photoreceptor ablation in the foveola.

It is important to note that the acute photoreceptor ablation model used in this study is distinct from genetic models of progressive retinal degeneration and should be viewed as complementary rather than an attempt to mimic the complex diseased state. The laser ablation approach allows us to tease apart the impact of the loss of photoreceptor signaling from other degenerative changes like compromised metabolic function. It also permits direct comparison of deafferented RGCs with healthy retina in the same eye, at the same time point. It does, however, bring other challenges; for example, inflammatory processes provoked by localized laser ablation may be different from those in naturally occurring retinal degenerations, and as the underlying pathology is absent, toxic changes in the retinal microenvironment due to the accumulation of undesirable metabolites, etc. are less likely to occur. The timescales for acuate later ablation versus progressive photoreceptor loss that may be sporadic and evolve over decades are also very different. Our results extend only to the 1 year time point in this simplified case. To date, there are no widely available genetic models of retinal degeneration in primates, although recent discoveries of naturally occurring retinal degenerations[26] in primates may make these models more widely available in the future. A strength of using a laser ablation approach versus the genetic models discovered to date is that it can be performed in the adult primate when the critical period is over, a situation more similar to retinal degenerations that develop in later life such as AMD.

Independent of the impact of deafferentation, we note that we were able to record optogenetic-mediated calcium responses from RGCs in animal 2 that had been expressing ChrimsonR-tdTomato and GCaMP for 2 years. This result in primate fovea is promising for optogenetic therapy as a stable treatment in patients. To generate high levels of transduction and long-term expression of our transgenes we used a relatively high viral vector dose (Table S2) relative to current clinical trials and paired this with immune suppression using cyclosporine A. Even with this immune suppression, we observed intraocular inflammation develop at 7 and 3 weeks after injection in animals 1 and 2, respectively, that was successfully treated with a single intravitreal steroid injection. A full characterization of the inflammatory response was beyond the scope of this paper, but given the relatively late time point, it is possible this represents an adaptive immune response to one or both transgenes. Despite this inflammation, viable expression was maintained for the course of the study. Further work is needed to establish whether the use of neuron-specific rather than ubiquitous promoters would negate the need for immune suppression with high-dose viral vector injections.

Studies of GCaMP3 in mouse brain have reported that high levels of GCaMP expression can be cytotoxic to neurons.[27] In this study optogenetic responsivity of RGCs with photoreceptor input intact remained relatively constant over the 3-month study period beginning 4.5 months after intravitreal injection of the viral vector (Figure 5). This finding in animal 1 together with the result that responses could still be obtained 2 years after the onset of expression in animal 2 (Figure 6) suggests that GCaMP was relatively well tolerated in the primate eye. Histology of the GCL 2 years after injection (Figure 7) also showed relatively normal cellular structure, although it is possible that subcellular signs of stress were present. To ensure that the long-term impact of deafferentation could be assessed independent of any effects of long-term GCaMP expression, we designed the study to measure relative changes in responsivity over time between deafferented RGCs and RGCs with photoreceptor input intact in an eccentricity-matched location in the same eye. This approach meant that any long-term changes due to GCaMP toxicity would impact both the deafferented and control groups and similarly ensured that the findings were robust to any day-to-day variability in AOSLO imaging performance.

These results demonstrate that 1 year after photoreceptor loss deafferented RGCs can support optogenetic-mediated activity at levels similar to optogenetic responses in intact retina. Although more work remains to understand the consequences of changes in protein expression, these results are promising for all vision restoration therapies that rely on preservation and reactivation of RGCs. Although we used calcium activity as a proxy for RGC function at the retinal level in this study, ultimately, to understand the impact of the observed changes on visual performance, psychophysical testing will be required.

MATERIALS AND METHODS

Animal care

The two macaques involved in this study were pair housed in an animal facility accredited by the Assessment and Accreditation of Laboratory Animal Care committee and cared for by 4 full-time veterinarians, 5 veterinary technicians, and an animal behaviorist from the Department of Comparative Medicine. The macaques had access to a complete nutritious chow and water *ad libitum* and were provided with additional green vegetables, trail mix, and other treats. Animal care staff monitored each animal for signs of discomfort at least twice every day. All animals had daily access to 2–4 pieces of manipulata such as mirrors and puzzle feeders and were frequently played music and movies. They received a weekly novel enrichment item, for example, treat-filled bags, eggs, grass, snow, maple branches, etc., together with rotating access to a larger play space with swings and elevated perches. This study was carried out in strict accordance with the Association for Research in Vision and Ophthalmology (ARVO) Statement for the Use of Animals and the recommendations in the *Guide for the Care and Use of Laboratory Animals* of the National Institutes of Health.

Co-expression of GCaMP6s and tdTomato-labeled ChrimsonR

AAV2-*CAG-tdTomato-ChrimsonR* and AAV2-*CAG-GCaMP6s*, synthesized by the University of Pennsylvania vector core, were intravitreally injected into the left eye of one male and the right eye of one female *Macaca fascicularis*. The eye was sterilized with 50% diluted Betadine before the vector was injected into the middle of the vitreous at a location ~3 mm behind the limbus with a 30-gauge needle with a tuberculin syringe. Neutralizing antibodies to AAV2 were measured in serum prior to purchase of monkeys and are expressed as the maximum serum dilution at which an antibody response is seen.

For both monkeys no antibody response was seen at the minimal dilution, 1:5. Both animals received daily subcutaneous cyclosporine A injections to suppress the immune system prior to and after injection of the viral vectors. A starting dose of 6 mg/kg was titrated into a therapeutic range of 150–200 ng/mL by monitoring blood trough levels. Once the desired blood trough level was achieved, that dose was adopted for several months after injection of the viral vector. The duration of immune suppression, injected titers, volumes, and animal details corresponding to each eye in the study are detailed in Table S2. Signs of intraocular inflammation were monitored by slit lamp examination, fundus photography, and observation of the pupillary response. The level of inflammation in animal 1 was graded weekly by an ophthalmologist for 8 weeks after injection of the viral vector, using the modified McDonald-Hackett scale. These data are shown in Table S1. Inflammation was treated by a single intravitreal injection of 50 μL of triamcinolone acetonide in formulation as either Triesence (animal 1) or Kenalog (animal 2), 8 and 3 weeks after injection of the viral vector, respectively, without subsequent recurrence. Immune suppression of animal 1 was halted after 9 months because of a loss of body condition.

Photoreceptor ablation

To remove photoreceptor input to a patch of RGCs, a 0.87° × 0.79° retinal region close to the central fovea was exposed for 106 ms to a scanning 55-fs pulsed 730-nm laser, with an average power of 4.48 Wcm^{-2} and a repetition rate of 80 MHz. The exposure was delivered to the photoreceptor layer with an adaptive optics scanning light ophthalmoscope.[28] This method of photoreceptor ablation offers enhanced lateral and axial confinement of the lesion and is described in detail elsewhere.[17] Because at the fovea RGCs are displaced from the photoreceptors that drive them, the lesion was also displaced and therefore the RGCs were not directly exposed to the ultrafast laser. The delivery of high-intensity pulsed NIR light through an adaptive optics system has previously been used to selectively ablate the photoreceptor layer in stem cell transplant studies[29] and optogenetics.[16,29]

Fundus imaging/OCT/cSLO imaging

Each eye in this study was imaged weekly with a conventional scanning light ophthalmoscope (Heidelberg Spectralis), OCT, and a fundus camera both prior to and after photoreceptor ablation. Animals were sedated with ketamine and medetomidine, and a contact lens was applied to the eye. The structural impact of the exposure was assessed with OCT. SLO 488-nm imaging with the blue autofluorescence modality was used to identify a region of reduced fluorescence providing a preliminary indication of ganglion cells that had been functionally impacted by photoreceptor damage. A fundus camera (Topcon TRC 50ex) equipped with custom filters to spectrally separate tdTomato from GCaMP6s (excitation 549/25 nm and emission 586/20 nm) was used to monitor expression levels of tdTomato-ChrimsonR independently. High-resolution structural and functional testing to assess the impact of the lesion was then conducted by AOSLO as described in the following sections. After imaging, anesthesia was reversed with an injection of Antisedan.

Adaptive optics scanning laser ophthalmoscopy

Animals were prepared for imaging as described previously.[16] Data were collected with an AOSLO system described in Gray et al.[30] Briefly, a Shack-Hartman wavefront sensor and deformable mirror were used to correct aberrations in closed loop with an 843-nm laser diode source (Thorlabs). A 796-nm superluminescent diode light source (Superlum) was focused on the photoreceptor layer, and reflectance images were collected with a 2 Airy disk pinhole at a rate of 25.6 Hz. A 488-nm laser source (Qioptiq) focused on the ganglion cell layer was used to excite GCaMP6s fluorescence and detected in a 517/20-nm emission band. An 8 Airy disk pinhole was used to maximize signal collection. The excitation light was presented only during the forward scan phase and filled the whole field except for experiments designed to stimulate photoreceptors, where the 488-nm imaging light was confined to the region of ganglion cell bodies and foveal photoreceptors were not exposed. The 488-nm imaging light intensities used were 7.6 $mWcm^{-2}$ in Figures 6F and 6G and 1.32 $mWcm^{-2}$ in all other cases.

Visual stimulation

The visual stimuli and imaging fields were stabilized on the retina with an approach described previously.[31] To drive ChrimsonR, a spatially localized, 640-nm, 0.45-Hz square wave drifting grating stimulus was focused onto the ganglion cell layer with a laser delivered through our 25.6-Hz AOSLO. Mean luminance of the stimulus was 50 mW cm^{-2} in Figures 6F and 6G and 28 $mWcm^{-2}$ in all other figures. The drifting grating stimulus was generated by modulating the intensity of the scanned laser source, creating a grating pattern moving at 0.45 Hz. After a 30-s period of adaptation to the 488-nm imaging light, the 640-nm optogenetic stimulus was presented for 90 s. To assess photoreceptor mediated activity, a 561-nm, 1 cycle/°, mean intensity 0.9 $mWcm^{-2}$, 0.45-Hz drifting grating was focused onto the photoreceptor layer in the central foveola.

Experimental design

To evaluate the impact of the loss of photoreceptor input on RGC responsivity, it was necessary to separate the impact of variable GCaMP expression levels over time and varying imaging parameters such as changes in fluorescence detection efficiency, slight variations in focal plane, etc. To mitigate the impact of these sources of variation, the response metric chosen was the sensitivity index (D′), which measures the detectability of the signal at the frequency of interest above the noise in neighboring frequency bands. Optogenetic stimulation and recording was performed both in the region lacking photoreceptor input and in an eccentricity-matched location on the opposite side of the RGC ring with photoreceptor input intact. In this way it was possible to examine the specific impact of the lesion versus longitudinal changes due to other factors. The optogenetic stimulation trial was repeated 4 times in each location plus two controls every week in the same order, so that changing image quality over the course of the 6-h imaging session would not impact longitudinal data. Control trials consisted of the presentation of the 488-nm imaging light only for the duration of the trial, to ensure that the signal recorded at the stimulation frequency was dependent on optical

stimulation, and a stimulus-only condition to confirm that there was no detectable optical bleed through of the stimulation light into the detection channel.

Data analysis

For each field of view the tenth infrared reflectance frame in the reflectance video was used as a reference, and frame-to-frame image registration of all videos for that field of view was performed with a strip-based cross correlation method[31] to remove image translation due to eye motion *in vivo*. Each frame of the fluorescence videos was co-registered with the high signal-to-noise infrared reflectance video captured simultaneously. Frames were summed to create reflectance images of the region of photoreceptor ablation and fluorescence images of the GCL in the two regions of interest. RGCs were segmented by hand in each to create a mask that could be applied to all videos recorded with that field of view. To track the same group of cells across multiple weeks, a master mask was translated and rotated to match the same region in each image. The master mask was created from the week 3 data for the area lacking photoreceptor input and from week 4 data for the RGCs with photoreceptors intact.

The frames corresponding to the 30-s adaptation period were removed from the registered fluorescence video, and the segmentation mask was applied to the remaining frames. The mean of the signal within each cell mask was computed for each frame, and a Hann windowing function was applied to the data. Each data sequence was temporally Fourier transformed into the frequency domain. The Fourier amplitudes were normalized by subtracting the mean and dividing by the standard deviation of the noise in the Fourier amplitudes in the ranges 0.75 Hz to 0.2 Hz and 0.7 Hz to 0.85 Hz and to avoid the optogenetic stimulation and respiration frequency and harmonics. This produced a response metric equivalent to the sensitivity index D′ and allowed comparison of optogenetic response detectability over time despite changing levels of GCaMP. To estimate the level of GCaMP expression in the segmented cells, a fluorescence measurement in the absence of optogenetic activity was needed. To achieve this, we Fourier transformed the last 20 s of the 30-s adaptation period for each trial in which no stimulus was presented. The amplitude of the first Fourier component (F0) at 0 Hz was used as a measure of the baseline fluorescence in the absence of stimulation.

To estimate the reduction of tdTomato fluorescence in the region of RGCs lacking photoreceptor input relative to those with photoreceptor input intact, measurements of the mean pixel intensity in fluorescent fundus images were made within the dark segment of deafferented RGCs and in an eccentricity-matched location. Images were co-aligned in Photoshop, converted to a stack, and analyzed in ImageJ[32] to compute a ratio of mean pixel values for each image.

Histology

Animal 2 was euthanized by an intravenous injection of Euthasol and perfused with 1 L of heparinized saline for 23 min and 1 L of 4% paraformaldehyde for 7 min. The right eye was enucleated, and the anterior segment was removed. The posterior segment was immersion fixed in 4% paraformaldehyde for 90 min. After fixation the tissue was washed twice for 5 min in PBS and cryoprotected in 10%, 20%, and 30% sucrose until equilibrated. Any adherent vitreous was removed from the retina. The tissue was embedded in OCT compound and frozen in isopentane cooled in liquid nitrogen. 20-μm frozen sections of retina were collected on Superfrost Plus slides and dried 60 min at 35°C on a slide warmer before being stored at −80°C. Sections within the lesion were identified with transmitted light microscopy and processed for immunofluorescence immunohistochemistry. Sections were blocked in a solution containing 10% normal horse serum, 1% Triton X-100, 0.025% NaN_3 in PBS for 1 h. Primary antibodies were diluted in 3% normal horse serum, 1% Triton X-100, 0.025% NaN_3 in PBS and applied overnight at 22–23°C. The following primary antibodies were used: rabbit anti-cone arrestin (LUMlf-hCAR, gift from Dr. Cheryl M. Craft, USC ROSKI Eye Institute and Keck School of Medicine of USC, 31, dilution 1:20,000), guinea pig anti-RBPMS (PhosphoSolutions, cat# 1832-RBPMS, dilution 1:500, Figure 7G, RRID: AB_2492226), rabbit anti-RBPMS (PhosphoSolutions, cat# 1830-RBPMS, dilution 1:500, Figure 7F, RRID: AB_2492225), guinea pig anti-VGLUT1 (EMD Millipore, cat# AB5905, dilution 1:5,000, RRID: AB_2301751). Secondary antibodies conjugated to Alexa 488, 594, or 647 (Invitrogen) were raised in goat or donkey and diluted 1:800 in 3% normal horse serum, 0.025% NaN_3 in PBS. Samples were mounted in Mowiol. Immunofluorescence samples were imaged on a laser scanning confocal microscope (Zeiss LSM 880) equipped with 488-, 561-, 594-, and 633-nm laser lines using a Zeiss Plan-Apochromat 20×/1.0 N.A. water or 60×/1.4 N.A. oil immersion objective. Image resolution was 1,024 × 1,024 pixels, and z axis step size was 1.2–1.5 μm for 20× images. Tiled image stacks were projected and stitched together in Zen 2 software. Brightfield images of toluidine blue/basic fuchsin (Multiple Stain Solution, #08824 Polysciences)-labeled sections were acquired with a Zeiss Axiocam MR digital camera on a Zeiss Axioskop microscope with a 40×/0.75 N.A. air objective. RGB channels were acquired separately through fluorescein isothiocyanate (FITC) (Ex 495 nm/ Em 519 nm), rhodamine (Ex 560 nm/Em 625), and Cy5 (Ex 650 nm/ Em 668 nm) filter sets and merged to generate RGB composite images. Overlapping image tiles were stitched together with the grid/collection stitching plugin[33] and adjusted for brightness and contrast with ImageJ.

Study approval

All protocols were approved by the University Committee on Animal Resources of the University of Rochester [PHS assurance number: D16-00188(A3292-01)].

SUPPLEMENTAL INFORMATION

Supplemental information can be found online at https://doi.org/10.1016/j.ymthe.2021.09.014.

ACKNOWLEDGMENTS

The authors wish to thank Amber Walker for assistance with animal care and anesthesia, Thurma McDaniel for tissue preparation for

immuno-histochemistry, and Qiang Yang, who developed image acquisition, stabilization, and registration software. We thank Kamal Dhakal for providing training and Jennifer Hunter and Khang Huynh for accommodating access to the 2P AOSLO. We thank Michael Giocomelli, Krystel Huxlin, and Louis DiVincenti for helpful discussions and Ron Plotnik and David DiLoreto, Jr. for providing clinical advice. We thank Erin Tepesch and Ying Kai Chan for assistance with characterizing inflammation. We thank the vector core at the Perelman School of Medicine, University of Pennsylvania and the Genetically-Encoded Neuronal Indicator and Effector (GENIE) Project and the Janelia Research Campus of the Howard Hughes Medical Institute, specifically Vivek Jayaraman, PhD, Douglas S. Kim, PhD, Loren L. Looger, PhD, and Karel Svoboda, PhD. This work was supported by the National Eye Institute (https://nei.nih.gov/about) through grants NIH EY021166 (to W.H.M), NIH EY025497 (to D.R.W.), and NIH EY024265 (to T.P.) and P30 Core Grants NIH EY001319 (University of Rochester) and NIH EY003176 (UC Berkeley) and through an unrestricted grant to the Flaum Eye Institute from Research to Prevent Blindness (https://www.rpbusa.org/rpb/grants-and-research/grants/rpb-unrestricted-grants/rpb-unrestricted-grants/). Confocal imaging was conducted in at the CRL Molecular Imaging Center at UC Berkeley (RRID:SCR_017852), supported by the Helen Wills Neuroscience Institute. We thank Holly Aaron and Feather Ives for microscopy assistance

AUTHOR CONTRIBUTIONS

J.E.M. designed and performed the experiments, developed and performed data analysis, interpreted results, managed the project, presented data, and wrote the manuscript. K.K. performed ultrafast laser exposures. Z.X. assisted with data analysis. P.J.M and T.G. assisted with data collection and analysis. K.P developed analysis routines. J.M.S. provided animal support. B.A.B. performed fluorescence fundus, OCT, and cSLO imaging. W.S.F. customized the fundus camera and performed OCT and cSLO. C.J.C. assessed intraocular inflammation. T.P. designed and performed immuno histochemistry and microscopy, interpreted results, and revised the manuscript. D.R.W. secured funding, interpreted results, and revised the manuscript. W.H.M. conceived the study, secured funding, interpreted results, performed intravitreal injections, revised the manuscript, and supervised the project.

DECLARATION OF INTERESTS

D.R.W. has received income in the form of royalties in excess of $10,000 from licenses on patents upon which he is an inventor, held by the University of Rochester. These patents have been awarded for wavefront sensing and adaptive optics technology, both of which were used to carry out the research described in this paper. He has also received research support in excess of $50,000 in the prior fiscal year from a company in a health care field. The nature of this research is completely unrelated to the subject matter or methods of the present publication. All other authors declare no competing interests.

REFERENCES

1. Pfeiffer, R.L., Marc, R.E., and Jones, B.W. (2020). Persistent remodeling and neurodegeneration in late-stage retinal degeneration. Prog. Retin. Eye Res. *74*, 100771.
2. Ogawa, S., Takemura, H., Horiguchi, H., Terao, M., Haji, T., Pestilli, F., Yeatman, J.D., Tsuneoka, H., Wandell, B.A., and Masuda, Y. (2014). White matter consequences of retinal receptor and ganglion cell damage. Invest. Ophthalmol. Vis. Sci. *55*, 6976–6986.
3. Boucard, C.C., Hernowo, A.T., Maguire, R.P., Jansonius, N.M., Roerdink, J.B.T.M., Hooymans, J.M.M., and Cornelissen, F.W. (2009). Changes in cortical grey matter density associated with long-standing retinal visual field defects. Brain *132*, 1898–1906.
4. Beyeler, M., Rokem, A., Boynton, G.M., and Fine, I. (2017). Learning to see again: biological constraints on cortical plasticity and the implications for sight restoration technologies. J. Neural Eng. *14*, 051003.
5. Strettoi, E., Pignatelli, V., Rossi, C., Porciatti, V., and Falsini, B. (2003). Remodeling of second-order neurons in the retina of rd/rd mutant mice. Vision Res. *43*, 867–877.
6. Margolis, D.J., Newkirk, G., Euler, T., and Detwiler, P.B. (2008). Functional stability of retinal ganglion cells after degeneration-induced changes in synaptic input. J. Neurosci. *28*, 6526–6536.
7. Mazzoni, F., Novelli, E., and Strettoi, E. (2008). Retinal ganglion cells survive and maintain normal dendritic morphology in a mouse model of inherited photoreceptor degeneration. J. Neurosci. *28*, 14282–14292.
8. Kolomiets, B., Dubus, E., Simonutti, M., Rosolen, S., Sahel, J.A., and Picaud, S. (2010). Late histological and functional changes in the P23H rat retina after photoreceptor loss. Neurobiol. Dis. *38*, 47–58.
9. Marc, R.E., Jones, B.W., Watt, C.B., Vazquez-Chona, F., Vaughan, D.K., and Organisciak, D.T. (2008). Extreme retinal remodeling triggered by light damage: implications for age related macular degeneration. Mol. Vis. *14*, 782–806.
10. Jones, B.W., Pfeiffer, R.L., Ferrell, W.D., Watt, C.B., Marmor, M., and Marc, R.E. (2016). Retinal remodeling in human retinitis pigmentosa. Exp. Eye Res. *150*, 149–165.
11. Jones, B.W., Pfeiffer, R.L., Ferrell, W.D., Watt, C.B., Tucker, J., and Marc, R.E. (2016). Retinal Remodeling and Metabolic Alterations in Human AMD. Front. Cell. Neurosci. *10*, 103.
12. Santos, A., Humayun, M.S., de Juan, E., Jr., Greenburg, R.J., Marsh, M.J., Klock, I.B., and Milam, A.H. (1997). Preservation of the inner retina in retinitis pigmentosa. A morphometric analysis. Arch. Ophthalmol. *115*, 511–515.
13. Denlinger, B., Helft, Z., Telias, M., Lorach, H., Palanker, D., and Kramer, R.H. (2020). Local photoreceptor degeneration causes local pathophysiological remodeling of retinal neurons. JCI Insight *5*, 132114.
14. Wan, J., Zheng, H., Hu, B.-Y., Xiao, H.-L., She, Z.-J., Chen, Z.-L., and Zhou, G.-M. (2006). Acute photoreceptor degeneration down-regulates melanopsin expression in adult rat retina. Neurosci. Lett. *400*, 48–52.
15. Stasheff, S.F. (2008). Emergence of sustained spontaneous hyperactivity and temporary preservation of OFF responses in ganglion cells of the retinal degeneration (rd1) mouse. J. Neurophysiol. *99*, 1408–1421.
16. McGregor, J.E., Godat, T., Dhakal, K.R., Parkins, K., Strazzeri, J.M., Bateman, B.A., Fischer, W.S., Williams, D.R., and Merigan, W.H. (2020). Optogenetic restoration of retinal ganglion cell activity in the living primate. Nat. Commun. *11*, 1703.
17. Dhakal, K.R., Walters, S., McGregor, J.E., Schwarz, C., Strazzeri, J.M., Aboualizadeh, E., Bateman, B., Huxlin, K.R., Hunter, J.J., Williams, D.R., and Merigan, W.H. (2020). Localized Photoreceptor Ablation Using Femtosecond Pulses Focused With Adaptive Optics. Transl. Vis. Sci. Technol. *9*, 16.
18. Dalkara, D., Kolstad, K.D., Caporale, N., Visel, M., Klimczak, R.R., Schaffer, D.V., and Flannery, J.G. (2009). Inner limiting membrane barriers to AAV-mediated retinal transduction from the vitreous. Mol. Ther. *17*, 2096–2102.
19. Dalkara, D., Byrne, L.C., Klimczak, R.R., Visel, M., Yin, L., Merigan, W.H., Flannery, J.G., and Schaffer, D.V. (2013). In Vivo–Directed Evolution of a New Adeno-Associated Virus for Therapeutic Outer Retinal Gene Delivery from the Vitreous. Sci. Transl. Med. *5*, 189ra76.
20. Drasdo, N., Millican, C.L., Katholi, C.R., and Curcio, C.A. (2007). The length of Henle fibers in the human retina and a model of ganglion receptive field density in the visual field. Vision Res. *47*, 2901–2911.
21. Rodriguez, A.R., de Sevilla Müller, L.P., and Brecha, N.C. (2014). The RNA binding protein RBPMS is a selective marker of ganglion cells in the mammalian retina. J. Comp. Neurol. *522*, 1411–1443.

22. Sakamoto, K., Liu, C., and Tosini, G. (2004). Classical photoreceptors regulate melanopsin mRNA levels in the rat retina. J. Neurosci. *24*, 9693–9697.

23. Yee, C.W., Toychiev, A.H., and Sagdullaev, B.T. (2012). Network deficiency exacerbates impairment in a mouse model of retinal degeneration. Front. Syst. Neurosci. *6*, 8.

24. Sekirnjak, C., Jepson, L.H., Hottowy, P., Sher, A., Dabrowski, W., Litke, A.M., and Chichilnisky, E.J. (2011). Changes in physiological properties of rat ganglion cells during retinal degeneration. J. Neurophysiol. *105*, 2560–2571.

25. Telias, M., Denlinger, B., Helft, Z., Thornton, C., Beckwith-Cohen, B., and Kramer, R.H. (2019). Retinoic Acid Induces Hyperactivity, and Blocking Its Receptor Unmasks Light Responses and Augments Vision in Retinal Degeneration. Neuron *102*, 574–586.e5.

26. Peterson, S.M., McGill, T.J., Puthussery, T., Stoddard, J., Renner, L., Lewis, A.D., Colgin, L.M.A., Gayet, J., Wang, X., Prongay, K., et al. (2019). Bardet-Biedl Syndrome in rhesus macaques: A nonhuman primate model of retinitis pigmentosa. Exp. Eye Res. *189*, 107825.

27. Tian, L., Hires, S.A., Mao, T., Huber, D., Chiappe, M.E., Chalasani, S.H., Petreanu, L., Akerboom, J., McKinney, S.A., Schreiter, E.R., et al. (2009). Imaging neural activity in worms, flies and mice with improved GCaMP calcium indicators. Nat. Methods *6*, 875–881.

28. Sharma, R., Schwarz, C., Williams, D.R., Palczewska, G., Palczewski, K., and Hunter, J.J. (2016). In Vivo Two-Photon Fluorescence Kinetics of Primate Rods and Cones. Invest. Ophthalmol. Vis. Sci. *57*, 647–657.

29. Aboualizadeh, E., Phillips, M.J., McGregor, J.E., DiLoreto, D.A., Jr., Strazzeri, J.M., Dhakal, K.R., Bateman, B., Jager, L.D., Nilles, K.L., Stuedemann, S.A., et al. (2020). Imaging Transplanted Photoreceptors in Living Nonhuman Primates with Single-Cell Resolution. Stem Cell Reports *15*, 482–497.

30. Gray, D.C., Wolfe, R., Gee, B.P., Scoles, D., Geng, Y., Masella, B.D., Dubra, A., Luque, S., Williams, D.R., and Merigan, W.H. (2008). In vivo imaging of the fine structure of rhodamine-labeled macaque retinal ganglion cells. Invest. Ophthalmol. Vis. Sci. *49*, 467–473.

31. McGregor, J.E., Yin, L., Yang, Q., Godat, T., Huynh, K.T., Zhang, J., Williams, D.R., and Merigan, W.H. (2018). Functional architecture of the foveola revealed in the living primate. PLoS ONE *13*, e0207102.

32. Schneider, C.A., Rasband, W.S., and Eliceiri, K.W. (2012). NIH Image to ImageJ: 25 years of image analysis. Nat. Methods *9*, 671–675.

33. Preibisch, S., Saalfeld, S., and Tomancak, P. (2009). Globally optimal stitching of tiled 3D microscopic image acquisitions. Bioinformatics *25*, 1463–1465.